Role of chemical disorder in slowing down diffusion in complex concentrated alloys

Shi-Cheng Dai [1,2] Yong Yang,[3,*] and Yun-Jiang Wang [1,2,†]

[1]*State Key Laboratory of Nonlinear Mechanics, Institute of Mechanics, Chinese Academy of Sciences, Beijing 100190, China*
[2]*School of Engineering Science, University of Chinese Academy of Sciences, Beijing 101408, China*
[3]*Department of Mechanical Engineering, College of Engineering, City University of Hong Kong, Tat Chee Avenue,*
Kowloon Tong, Kowloon, Hong Kong SAR, China

The advent of multiprincipal element alloys (MPEAs) has sparked significant interest in physical metallurgy. These alloys, distinguished by their high configurational entropy aimed at minimizing free energy, have raised intriguing questions regarding the interplay of chemical disorder and chemical short-range order (CSRO) in kinetics of MPEAs. Particularly, the widely assumed phenomenon of sluggish diffusion has come under scrutiny. Here we employ atomistic simulations to quantitatively evaluate the impact of CSRO on diffusion in a representative medium-entropy alloy. We introduce a physical order parameter to establish a quantitative correlation between CSRO and diffusivity. Surprisingly, our simulations suggest that CSRO, rather than chemical disorder, serves to suppress and localize defect diffusion. The observed link between diffusion activation energy and CSRO provides a rationale for the observed deceleration in diffusion due to chemical ordering. A linear relationship between diffusion activation energy and activation entropy is unveiled, aligning with the Meyer-Neldel rule, and replicating experimental results. These insights help clarify the intricate role of chemical disorder in plastic deformation of chemically disordered materials.

I. INTRODUCTION

Traditional metallic alloys historically involved adding dilute concentrations of alloying elements to a base metal. However, in the past decade, there has been a transformative shift in alloy design philosophy, focusing on exploring the central region of multicomponent compositional space. This innovative concept, known as chemically complex concentrated alloys, multiprincipal element alloys (MPEAs), or more commonly, medium- to high-entropy alloys (HEAs) [1–3], depending on the number of constituent elements, has garnered significant attention in the fields of materials science and condensed matter physics. MPEAs, often forming highly concentrated single-phase solid solutions due to their elevated configurational entropy, exhibit a plethora of exceptional mechanical and functional properties [4–10].

In the early stages of research, the prevailing notion was that these alloys featured a random local environment, and this led to the assumption of maximum configurational entropy for phase stability. However, recent experimental and simulation findings challenge this conventional wisdom by unveiling the presence of chemical heterogeneity within these multiconstituent alloys. This heterogeneous spatial distribution of elements results in the segregation of specific elements and the emergence of chemical short-range order (CSRO). It has become increasingly evident that CSRO exerts a profound influence on the deformation mechanisms, strength,

and ductility of MPEAs [11–16]. More recently, advanced techniques such as atomic-resolution energy-dispersive x-ray spectroscopy and energy-filtered transmission electron microscopy have enabled the direct observation of this local chemical heterogeneity and exploration of its role in deformation physics of these complex materials [17,18].

With the growing recognition of CSRO, it is natural to consider an important transport phenomenon—diffusion, which plays a crucial role in the plastic deformation of solids. Diffusion is a fundamental process that greatly influences various material properties, including creep resistance, radiation tolerance, phase transitions, and mechanical behaviors at elevated temperatures [19]. Notably, all these properties are profoundly affected by local chemical fluctuations [19–21]. Although the concept of sluggish diffusion was initially proposed as a core effect of HEAs, a unanimous consensus on the applicability of sluggish diffusion to all systems or elements within HEAs remains elusive [22–25]. Nonetheless, this concept has ignited extensive fundamental research into diffusion in this new class of materials.

From a microscopic perspective, self-diffusion in pure crystalline metals, mediated by the random jump of vacancies, is well understood. However, due to the different jump probabilities of various species in MPEAs, local variation in chemical composition leads to distinct and path-dependent energy barriers, resulting in inherently biased jump probabilities [26]. Unfortunately, experimental methods for diffusion test often conflict with the CSRO. Holding these materials for several days at elevated temperatures (~1000–1300 K) typically yields nearly homogeneous alloys, diminishing the influence of CSRO on diffusion outcomes [27]. As a pivotal initial

---

*Corresponding author: yonyang@cityu.edu.hk
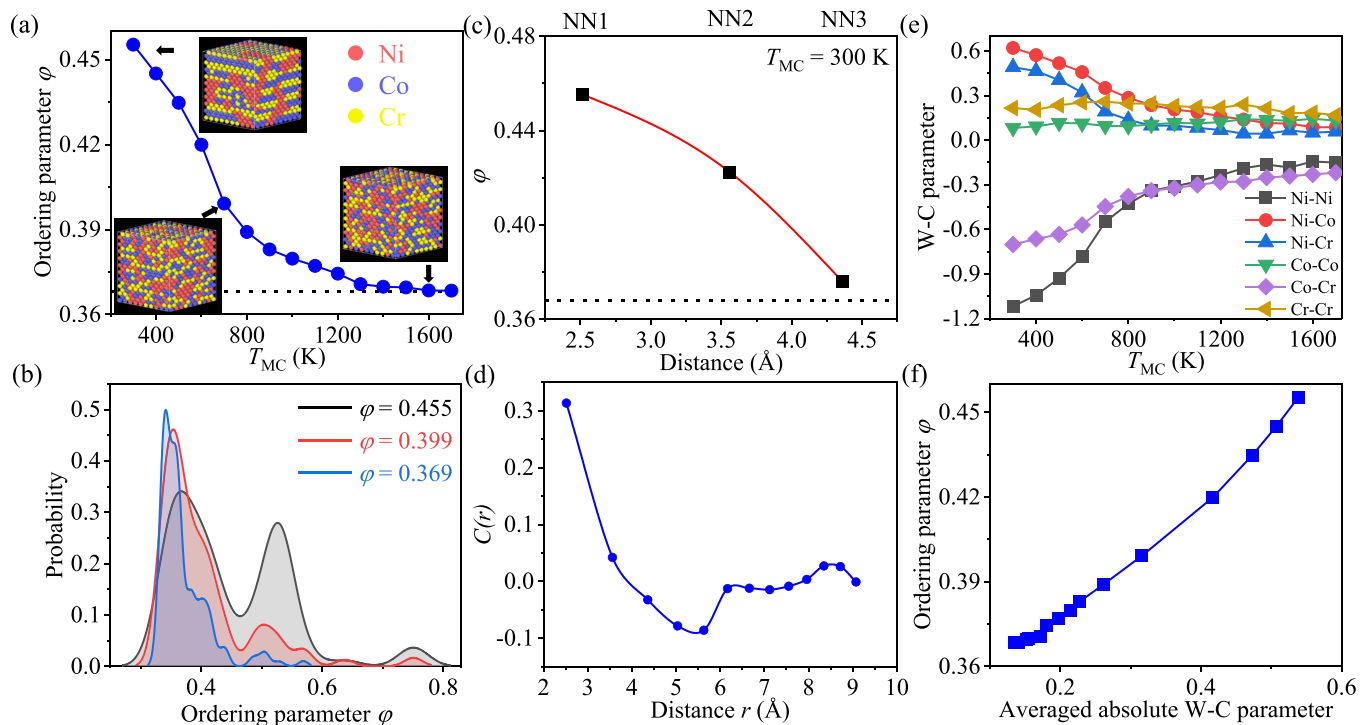†Corresponding author: yjwang@imech.ac.cn

FIG. 1. Emergence of chemical ordering. (a) Order parameter φ for samples prepared under different Monte Carlo temperature T_{MC}. Insets depict the corresponding atomic configurations. (b) Histograms representing the distribution of the order parameter in various configurational spaces. (c) φ calculated by considering varying levels of nearest neighbors. (d) Spatial autocorrelation functions of the order parameter. (e) Evolution of the Warren-Cowley parameters as a function of T_{MC}. (f) φ versus the averaged absolute values of the pairwise Warren-Cowley parameters.

step in comprehending the structure-property relationships, it becomes imperative to uncover all significant mechanisms at play, especially the role of CSRO within the first few nearest-neighbor atomic shells, and to define these mechanisms in physical terms.

Considering the characteristic size of chemical heterogeneity, molecular dynamics (MD) simulations offer an advantageous approach for exploring the relationship between diffusion and CSRO in a relatively clear state. Hybrid Monte Carlo (MC)/MD simulations have revealed that CSRO reduces and localizes vacancy-mediated diffusion in CrCoNi, MoNbTa [28], and CuNiCoFe MPEAs [29]. Machine learning methods, including convolutional neural networks, have successfully predicted path-dependent vacancy migration energy barrier spectra with various compositions in MoNbTa MPEAs [26,30]. However, these previous discussions have primarily adopted a qualitative perspective, necessitating further quantitative insights. Our efforts aim to establish a quantitative relationship between diffusivity and the extent of CSRO, thereby providing clarity to the ongoing debate surrounding sluggish diffusion in these complex materials.

In this study, we tackle this challenge by delving into the vacancy diffusion mechanism within a NiCoCr medium-entropy alloy using MD simulations. Utilizing a hybrid MC/MD approach, we construct models with varying degrees of CSRO, which exerts a decelerating effect on diffusion when compared to the fully disordered state. Chemical order leads to increased activation energy, consequently slowing down the kinetics. Notably, varying CSRO allows one to observe an

intriguing entropy-enthalpy compensation phenomenon within the kinetics of chemically disordered solids.

II. ATOMIC CHARACTERIZATION OF THE CSRO

A physical order parameter φ (at atomic scale) is used to characterize the degree of CSRO, which can be defined by the following equation:

$$\varphi = e^{\langle -s_i \rangle}, \tag{1}$$

where $s_i = -\sum x_A \ln x_A$ is the Shannon entropy of the i_{th} atom and x_A represents the concentration of element A in the nearest neighbors. Averaging over all the atoms in the configuration gives rise to a sample-level degree of CSRO. Figure 1 attempts to illustrate the applicability of the order parameter. Figure 1(a) shows how the φ is related to the configurations obtained by hybrid MC/MD modeling at different annealing temperatures (T_{MC}). The value of φ corresponding to the most ordered state and random disordered state is 0.455 and 0.368, which have been annealed sufficiently at 300 and 1650 K, respectively. A noteworthy trend is that φ decreases monotonically from the most ordered ($\varphi = 0.455$) to the random state ($\varphi = 0.368$) with increasing T_{MC}. The dashed line in Figs. 1(a) and 1(b) is the level of random solid solution. The trend is consistent with previous studies [11,12,17,18], which suggest that various CSRO persists across a wide range of T_{MC}.

Figure 1(b) shows a specific distribution of the atomic scale φ_i in configurations with different degree of the global chemical order φ. With decreasing φ, the distribution of φ_i changes

from multipeak nature to a single peak that corresponds to the state of fully chemical disorder, along with the narrowing of distribution. Interestingly, even in the most ordered configuration ($\varphi = 0.455$), a considerable fraction of atoms has small φ_i value comparable to random state. Meanwhile, even in the random disordered configuration a small number of atoms still have some chemical order with high φ_i. From distribution of φ_i, we illustrate why an ideal random or completely ordered MPEA solid solution is difficult to reach, as almost all observed configurations possess partial CSRO.

In Figs. 1(c) and 1(d), we examine the short-range characteristics of φ from two different perspectives: by considering different shells of nearest neighbors and by assessing the spatial correlation. Firstly, the order parameter φ mentioned above only considers the nearest neighbor, while in Fig. 1(c), additional shells including second nearest (NN2) and third nearest (NN3) neighbors are also included. As the distance increases to the third nearest neighbor, φ_i values rapidly decay to indicate a fully disordered state. Secondly, the spatial autocorrelation function of φ is calculated as follows:

$$C_\varphi(r) = \frac{\langle \Delta\varphi_{r_0} \Delta\varphi_{r_0+r} \rangle - \langle \Delta\varphi_{r_0} \rangle^2}{\langle \Delta\varphi_{r_0}{}^2 \rangle - \langle \Delta\varphi_{r_0} \rangle^2}. \quad (2)$$

Here $\Delta\varphi_{r_0} = \varphi_{r_0} - \varphi$ represents the deviation of φ for the ith atom at a reference position r_0 from the sample-averaged φ. Similarly, $\Delta\varphi_{r_0+r}$ is the deviation for the atoms that are r units away from the ith atom. The angle brackets denote the ensemble average. The calculated spatial autocorrelation function is presented in Fig. 1(d) as a function of the ith nearest-neighbor distance, extending up to the 13th nearest neighbor. The calculated spatial autocorrelation value ranges from −1 to 1. A positive value indicates positive spatial autocorrelation, suggesting that similar values tend to be clustered together. Conversely, a negative value indicates negative spatial autocorrelation, implying that dissimilar values are clustered together. A value close to zero indicates no spatial autocorrelation or randomness. As the distance increases to the third nearest neighbor, $C_\varphi(r)$ rapidly decays to values close to 0 and fluctuates around 0, indicating an uncorrelated state. Both the results of Fig. 1(c) and 1(d) confirm the short-range nature of the chemical order.

Moving forward, we emphasize the advantages of using this physical order parameter φ, which offers a convenient and quantitative means to measure the CSRO of the entire system in an easily manageable manner. To illustrate this point, we have computed the Warren-Cowley (W-C) parameter [31], a commonly used descriptor of CSRO, as shown in Fig. 1(e). Our results are consistent with those obtained by Li *et al.* [14], which is expected since both sets of results are based on the same interatomic potential. The W-C parameter is defined by the formula $\alpha_{ij} = 1 - \frac{p_{ij}}{c_i c_j}$, where p_{ij} is the probability of finding a j-type atom among the neighbors of the i-type atoms, and c_i, c_j are the concentrations of the corresponding elements. For a random model, α_{ij} is zero. For a specific pair, for example, Ni-Ni atomic pair, a negative α_{ij} suggests the tendency of j-type clustering around an i-type atom while a positive α_{ij} means the opposite. This parameter is applicable for describing the chemical order of a specific pair of elements. In a ternary system, six independent W-C parameters

are required to quantify the CSRO of the entire system, and for a quaternary system, ten are needed. In contrast, the order parameter φ provides a unique, universal measure regardless of the number of principal elements. Finally, we compare φ with the W-C parameters in an ensemble-average sense. Figure 1(f) presents a quantitative comparison between φ and the averaged absolute value of W-C parameters, denoted as $\bar{\alpha}$ ($\bar{\alpha} = \langle |\alpha_{ij}| \rangle$). The evolution trend of φ is in alignment with that of $\bar{\alpha}$, suggesting a complementary relationship between the order parameter and the commonly used W-C parameter. In summary, order parameter φ allows for the quantitative characterization of the overall degree of CSRO. Furthermore, we speculate that φ can also facilitate direct comparisons of CSRO among MPEAs with the same number of principal elements but different species.

III. EFFECT OF CSRO ON DIFFUSIVITY

To begin with, we present the results of thermally activated diffusivity for point defects within the alloy configurations. Figure 2 depicts the mean-squared displacement (MSD) curves for single vacancy migration. The slope of these curves increases with rising temperatures, consistent with the expected temperature-dependent effects on diffusion. Figure 2(b) illustrates MSD as a function of time at varying values of φ, while keeping temperatures constant. It is noteworthy that the slope of the MSD versus time decreases with increasing φ, indicating that CSRO hinders vacancy transport. Notably, Figs. 2(a) and 2(b) reveal that the vacancy diffusion process in the NiCoCr alloy follows a rugged MSD curve, a striking contrast to conventional metals like Cu where the MSD linearly evolves with time [32]. This observation is further illustrated by the regions colored blue in Fig. 2(c) with ΔMSD < 0 concerning the linear MSD with time, which restrict vacancy diffusion when vacancies enter these local regions. Conversely, diffusivity is enhanced when vacancies move into low-barrier regions, depicted in red with ΔMSD > 0 in Fig. 2(c). The vacancy diffusion in MPEAs is significantly more intricate, and intermittent vacancy progressions occur when soft and strong bonding regions alternate in distribution, as shown in Figs. 2(c) and 2(d). These findings underscore the substantial impact of CSRO on vacancy diffusion in MPEAs. CSRO not only impedes vacancy diffusion but also introduces complexity into the MSD curves, reflecting the rough potential energy landscape and atomic environment within MPEAs.

In a conventional fcc crystal, vacancies are equally likely to jump to any of the 12 first nearest-neighboring sites since there are no distinctions among them. However, in MPEAs, defect jumps are chemically biased due to restricted jump directions and trial frequencies. A typical example is depicted in Fig. 3, which illustrates diffusion trajectories for two models considered in this study: a random model ($\varphi = 0.369$) and an ordered model ($\varphi = 0.455$) over the same time intervals (1 ns), as shown in Figs. 3(a) and 3(b), respectively. In the random model shown in Fig. 3(b), the vacancy travels a relatively long distance, whereas in the ordered model shown in Fig. 3(a), diffusion becomes spatially constrained. The vacancy becomes trapped at certain sites for an extended period, adjusting itself for further diffusion. Consequently, the vacancy only covers a short distance before becoming
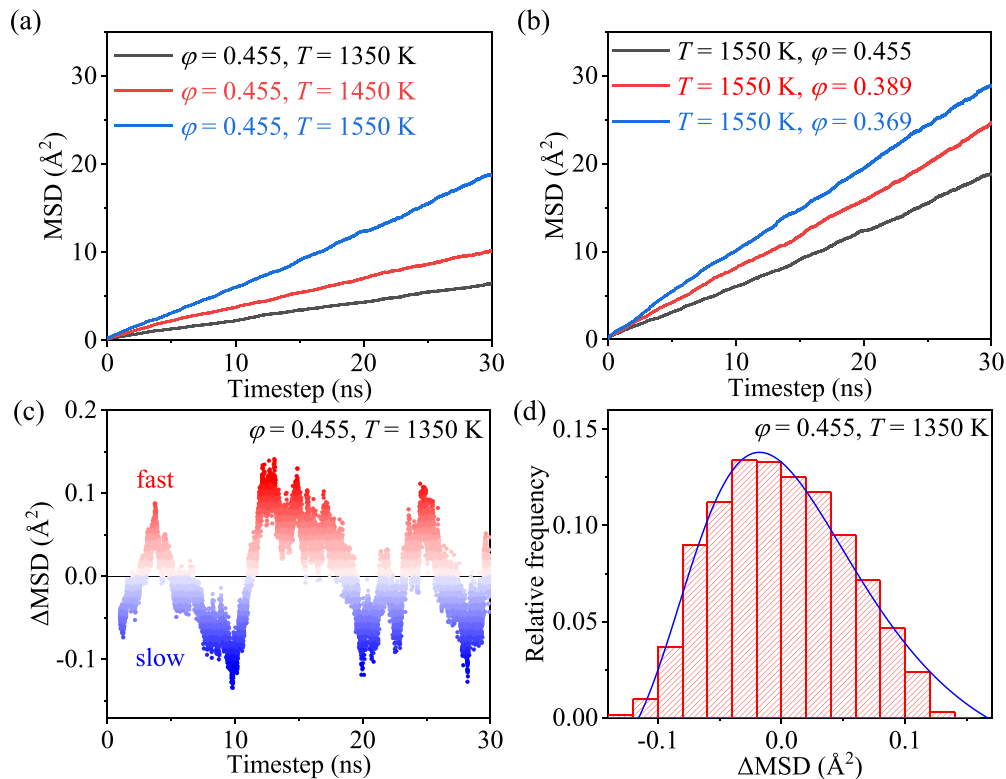
FIG. 2. Chemical order suppresses diffusion kinetics. (a) MSD versus time in the same configuration ($\varphi = 0.455$) at varying temperatures. (b) MSD for different samples (varying φ) at a fixed temperature (1550 K). (c) Residual MSD at $\varphi = 0.455$ and $T = 1350$ K, showing "fast" regions colored in red (ΔMSD > 0) and "slow" regions (ΔMSD < 0). Δ denotes deviation from linearity. (d) Asymmetric distribution of ΔMSD with $\varphi = 0.455$ and $T = 1350$ K, fitted by the extreme value distribution.

immobilized in the lattice near the starting point. This stark comparison illustrates how local chemical fluctuations can hinder defect motion, in agreement with MSD fluctuation shown in Fig. 2. Crucially, it highlights the pronounced effect of CSRO in localizing vacancy diffusion.

According to the Arrhenius equation, the kinetics of the thermally activated defect diffusion can be determined using the following equation:

$$D = D_0 \exp\left(\frac{-\Delta E}{k_\mathrm{B} T}\right). \tag{3}$$

Here, D represents the diffusion coefficient, D_0 is the prefactor of diffusion including geometrical and entropic factors, ΔE is the activation energy, k_B is the Boltzmann constant, and T is the absolute temperature. We directly obtain the diffusion coefficients of single vacancies from the plots in Fig. 2 using Eq. (5) in Appendix B (see the details of calculation methods in Appendix B). The results are presented in Fig. 4(a), considering three different states: the ordered ($\varphi = 0.455$), the partially ordered ($\varphi = 0.399$), and the random ($\varphi = 0.369$). In the atomic models, for vacancy diffusion, the diffusion coefficient D is the lowest in the ordered model across the
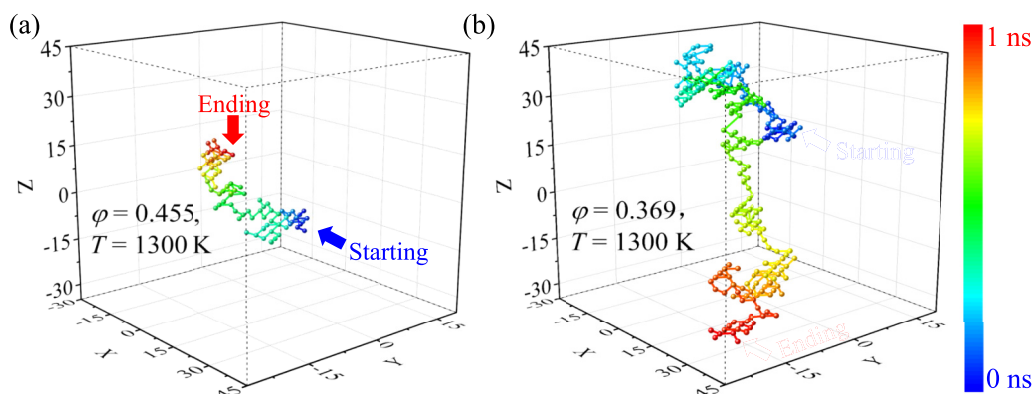

FIG. 3. Trajectories of vacancy diffusion for two specific configurations with $\varphi = 0.455$ (a) and $\varphi = 0.369$ (b) at 1300 K over a uniform time interval of 1 ns. Trajectories are color coded based on diffusion time. The starting and ending points are marked by blue and red arrows, respectively.
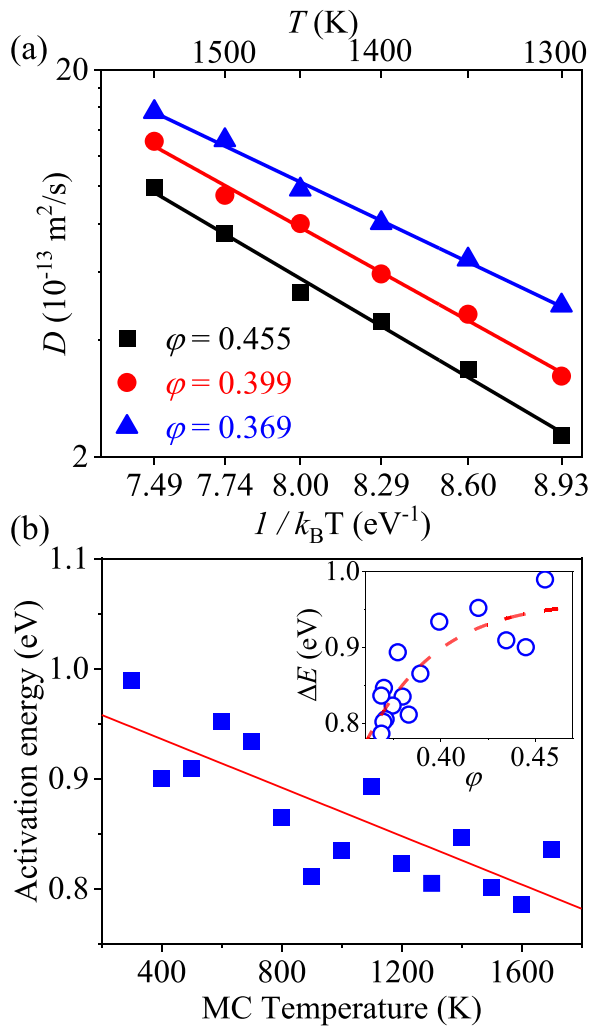
FIG. 4. (a) Arrhenius plot illustrating diffusivity for samples with different values of φ, encompassing ordered, partially ordered, and random alloys. (b) Activation energy versus annealing temperature T_{MC}. Inset displays the correlation between activation energy and the degree of CSRO φ.

FIG. 5. Correlation between diffusion prefactor D_0 and activation energy ΔE, indicating the existence of the Meyer-Neldel rule in MPEAs.

entire temperature range considered, followed by the partially ordered model, and finally the random model. The results clearly demonstrate that local chemical order suppresses vacancy diffusion in MPEAs. It is worth noting that values of D obtained through simulations are several orders of magnitude larger than those reported in experimental data [33]. This discrepancy is expected because the vacancy concentration in our model ($C = 2.5 \times 10^{-4}$) is significantly higher than the equilibrium vacancy concentration in the experimental sample, particularly at low temperatures. For example, if one calculates the equilibrium vacancy concentration using the average formation energy E_{f} ($= -1.67$ eV) as $C_{\mathrm{eq}} = \exp(\frac{-E_{\mathrm{f}}}{k_{\mathrm{B}}T})$ at $T = 1300$ K, the calculated value yields $C_{\mathrm{eq}} = 3.3 \times 10^{-7}$, which is orders of magnitude smaller than that in our atomic model.

To gain further insights into the influence of CSRO on diffusion, we also present the activation energies obtained from Arrhenius fitting in Fig. 4(b). In this presentation we use the Monte Carlo temperature as an indicator of CSRO
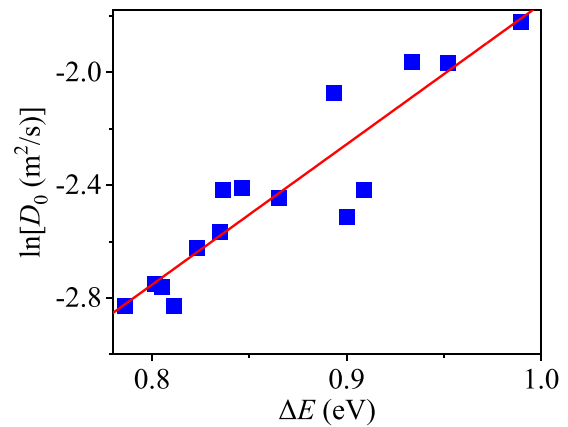
to clearly demonstrate the relationship between CSRO and diffusivity. As observed, this relationship exhibits a linearly descending trend, highlighting the inverse correlation between CSRO and activation energy. The inset provides an additional perspective by illustrating the relationship between activation energies and φ, revealing a nonlinear scaling relationship characterized by increasing activation energy with formation of chemical order. The observation of the CSRO's effect on activation energies aligns with our findings related to diffusion coefficients. Specifically, we note that the activation energy decreases as we progress from the ordered model to the partially ordered model and finally to the random model. Overall, CSRO renders vacancy diffusion energetically unfavorable, as evidenced by the highest activation energy in the ordered model. This increased activation energy has something to do with the enhanced dynamic heterogeneity in point defect diffusion, indicating reduced randomness. Considering the impact of CSRO on MSD, diffusion trajectories, and tracer diffusion coefficients, we conclude that CSRO indeed constrains and localizes defect diffusion. This restriction arises from the fact that the migration energy is elevated by the presence of local chemical order.

To delve further into the physical aspects, we turn our attention to the relationship between activation energy ΔE and the diffusion prefactor D_0, which is connected to entropy—an aspect seldom discussed in the limited literature but one that holds critical significance for diffusion in high-entropy materials. Through Arrhenius analysis, we have obtained a set of activation energies and prefactors in the calculations. Figure 5 presents a correlation plot between $\ln D_0$ and ΔE for NiCoCr systems with varying degree of CSRO. Remarkably, we observe a linear relationship, consistent with experimental measurements in a CoCrFeNi MPEA [34]. This linear scaling can be described as

$$\ln D_0 = (-6.74 \pm 0.50) + 4.97\Delta E. \qquad (4)$$

Here D_0 and ΔE are expressed in units of m^2/s and eV, respectively. The prefactor D_0 can generally be presented in the form $\ln D_0 = c + \frac{\Delta S}{k_{\mathrm{B}}}$, establishing a corresponding relationship between D_0 and the diffusion activation entropy (ΔS). The linear correlation implies that the configurational

disorder (via φ) is closely related to its vibrational counterpart (via thermal activation of diffusion) in MPEAs. This empirical linear relationship is known as the Meyer-Neldel rule (MN rule) or compensation law in multidisciplinary fields. It has been observed across a wide range of physical and chemical kinetic processes but has been rarely reported in deformation of MPEAs. Notably, the coefficient of ΔE in Eq. (4) corresponds to $1/k_B T_{MN}$, where T_{MN} denotes the Meyer-Neldel characteristic temperature. For NiCoCr, the value of T_{MN} is 2335 K, which is higher than the melting point.

The applicability of the MN rule indicates the existence of an empirical enthalpy-entropy compensation in kinetics of MPEAs, such as the NiCoCr system studied in this work. This correlation unveils a complex scenario in diffusion kinetics, where diffusivity is not solely determined by activation energy but instead a combined function of activation energy and the preexponential factor, which in turn depends on activation entropy (ΔS). As a result, it becomes imperative to give due consideration to ΔS in the description of diffusion kinetics of chemically complex crystals. Moreover, the MN rule implies that ΔS can be roughly approximated by $\Delta E/T_{MN}$, where the value of T_{MN} can serve as a reference for other thermally activated processes in materials. For instance, in our previous study of dislocation nucleation within the same NiCoCr system, we obtained a similar value of $T_{MN} = 2223$ K [35]. This suggests that different forms of plastic deformation in high-entropy materials may share similar physical origin in terms of thermodynamic characteristics.

IV. CONCLUSION

In summary, our investigation has delved into the impact of CSRO on point defect diffusion within a model NiCoCr MPEA through the application of hybrid MC/MD simulations. We have quantified the degree of CSRO through the introduction of a physical order parameter. By comparing MPEA configurations with varying levels of CSRO, we have revealed that vacancies tend to become trapped in low-energy regions, resulting in increased activation energy and localized diffusion trajectories. These observations underscore the inherent ruggedness of the potential energy landscapes within MPEAs due to their complex chemical environments. The atomistic simulations unequivocally demonstrate that CSRO exerts a suppressing and localizing effect on single vacancy diffusion, and this effect becomes more pronounced with increasing CSRO. This leads us to posit that the traditional potential energy landscape may not be adequate to elucidate the sluggish diffusion phenomenon in MPEAs, as CSRO can similarly contribute to this effect. Furthermore, our findings highlight an intriguing enthalpy-entropy compensation phenomenon, shedding light on the pivotal role of entropy in the materials kinetics of high-entropy alloys. These atomistic insights not only elucidate the critical role of chemical disorder in diffusion within crystalline MPEAs but also propose potential thermal processing strategies for tailoring the mechanical properties of these chemically complex materials. The annealing-temperature-dependent manipulation of CSRO emerges as an effective strategy for property control in MPEAs, offering avenues for materials design and optimization in this exciting class of alloys.

APPENDIX A: HYBRID MC/MD APPROACH

To prepare samples of CoCrNi with various degrees of CSRO, the hybrid MC/MD method is applied to the bulk material without the presence of any defect. The annealed cell is initially created with a random distribution of elements at the desired equimolar composition. Then the samples are annealed using a hybrid MC/MD approach. The Monte Carlo scheme mimics diffusion by allowing for an exchange of any pair of distinct species (a swap) inside the lattice, meanwhile the overall concentration is kept constant throughout. One MD operation (containing ten MD steps) under *NPT* conditions is inserted between two MC steps to relax any local residual stress due to the swaps in the system. By combining a MC
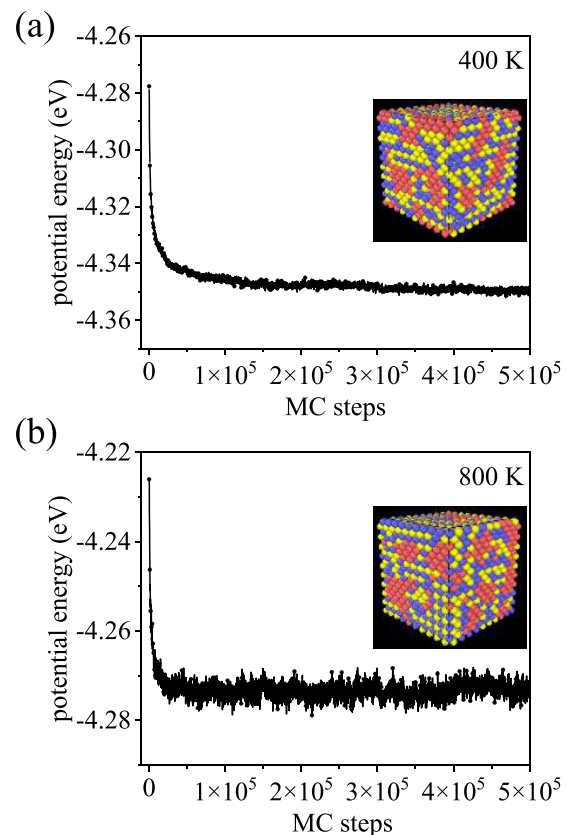

FIG. 6. Convergence of potential energy during the annealing procedure at 400 K (a) and 800 K (b), respectively.

interspecies move with MD, a representative structure at a fixed concentration isobaric-isotherm ensemble is obtained. By adjusting the annealing temperature of the hybrid MC/MD samples with specific Monte Carlo temperature T_{MC} (make a distinction of the real MD temperature in diffusion) varying from 300 to 1700 K, a total of 15 configurations with different extent of CSRO are prepared. To evaluate the convergence of the annealing procedure, we monitored the potential energy per atom as a function of the number of attempted swaps or simulation time (Fig. 6). The annealing process was concluded when a satisfactory level of convergence was achieved, typically after approximately 500 000 MC steps were attempted across the entire system.

Convergence testing confirms that a model size of 4000 atoms results in a reliable value of chemical order. In a larger model comprising 32 000 atoms, there is only a minor difference of less than 2%, with $\varphi = 0.4199$ for the 4000-atom model and $\varphi = 0.4119$ for the 32 000-atom model.

APPENDIX B: ATOMISTIC SIMULATION OF DIFFUSION

MD simulations were performed using the LAMMPS package [36]. A recently developed density functional theory calibrated embedded-atom potential for NiCoCr MPEA by Li *et al.* [14] is adopted to describe the empirical force fields. The periodic dimensions of the simulation cell in an fcc lattice use a simple orthogonal coordinate system such as $x = [100]$, $y = [010]$, $z = [001]$. Each dimension contains ten lattices, for a total of 4000 atoms in the simulation cell.

The diffusivity of an MPEA model is investigated by removing one atom within the cell randomly to produce a vacancy. The diffusion kinetics in NiCoCr models are performed over a wide temperature range of 1300–1550 K with intervals of 50 K. Before the measurement of diffusivity, all the cells were thermally equilibrated for 100 ps at each specific targeted temperature by using the Nose-Hoover thermostat within an isobaric-isothermal ensemble. Then MD simulation is performed for 40–60 ns, depending on the targeted temperature, which allows one to reach the effective diffusion coefficient [32]. The diffusivities are determined by linearizing a plot of MSD versus time, with the cutoff time where the linear relation has been well established. The slopes of these well-defined linear relations provide quantitative information for the diffusion coefficients by the Einstein relation:

$$D = \frac{\langle |\mathbf{r}(t) - \mathbf{r}(0)|^2 \rangle}{6t}, \qquad (B1)$$

where the numerator $\langle |\mathbf{r}(t) - \mathbf{r}(0)|^2 \rangle$ denotes MSD, and $\mathbf{r}(t)$ and $\mathbf{r}(0)$ are the positions of atoms at times t and $t = 0$, respectively. The MSD is shown as a function of time at different temperatures and different CSRO, respectively. The defect trajectory is recorded as a sequence of defect position after each jump. To extract diffusion trajectory, we locate the vacancy position at each step via the Wigner-Seitz defect analysis. The software OVITO is adopted to visualize the atomic configurations [37].

[1] J. W. Yeh, S. K. Chen, S. J. Lin, J. Y. Gan, T. S. Chin, T. T. Shun, C. H. Tsau, and S. Y. Chang, Nanostructured high-entropy alloys with multiple principal elements: Novel alloy design concepts and outcomes, Adv. Eng. Mater. **6**, 299 (2004).

[2] E. P. George, D. Raabe, and R. O. Ritchie, High-entropy alloys, Nat. Rev. Mater. **4**, 515 (2019).

[3] W. Li, D. Xie, D. Li, Y. Zhang, Y. Gao, and P. K. Liaw, Mechanical behavior of high-entropy alloys, Prog. Mater Sci. **118**, 100777 (2021).

[4] Y. Zhang, T. T. Zuo, Z. Tang, M. C. Gao, K. A. Dahmen, P. K. Liaw, and Z. P. Lu, Microstructures and properties of high-entropy alloys, Prog. Mater. Sci. **61**, 1 (2014).

[5] Z. Li, S. Zhao, R. O. Ritchie, and M. A. Meyers, Mechanical properties of high-entropy alloys with emphasis on face-centered cubic alloys, Prog. Mater. Sci. **102**, 296 (2019).

[6] Z. J. Zhang, M. M. Mao, J. Wang, B. Gludovatz, Z. Zhang, S. X. Mao, E. P. George, Q. Yu, and R. O. Ritchie, Nanoscale origins of the damage tolerance of the high-entropy alloy CrMnFeCoNi, Nat. Commun. **6**, 10143 (2015).

[7] W. M. Choi, Y. H. Jo, S. S. Sohn, S. Lee, and B. J. Lee, Understanding the physical metallurgy of the CoCrFeMnNi high-entropy alloy: An atomistic simulation study, npj Comput. Mater. **4**, 1 (2018).

[8] N. L. N. Broge, M. Bondesgaard, F. Søndergaard-Pedersen, M. Roelsgaard, and B. B. Iversen, Autocatalytic formation of high-entropy alloy nanoparticles, Angew. Chem., Int. Ed. **59**, 21920 (2020).

[9] J. J. Zhang, X. L. Yin, Y. Dong, Y. P. Lu, L. Jiang, T. M. Wang, and T. J. Li, Corrosion properties of Al$_x$CoCrFeNiTi$_{0.5}$ high entropy alloys in 0·5M H$_2$SO$_4$ aqueous solution, Mater. Res. Innovations **18**, S4756 (2014).

[10] X. T. Li, X. Z. Tang, Y. F. Guo, H. Li, and Y. Fan, Modulating grain boundary-mediated plasticity of high-entropy alloys via chemo-mechanical coupling, Acta Mater. **258**, 119228 (2023).

[11] R. Zhang, S. Zhao, J. Ding, Y. Chong, T. Jia, C. Ophus, M. Asta, R. O. Ritchie, and A. M. Minor, Short-range order and its impact on the CrCoNi medium-entropy alloy, Nature (London) **581**, 283 (2020).

[12] F. Walsh, M. Asta, and R. O. Ritchie, Magnetically driven short-range order can explain anomalous measurements in CrCoNi, Proc. Natl. Acad. Sci. USA **118**, e2020540118 (2021).

[13] J. Ding, Q. Yu, M. Asta, and R. O. Ritchie, Tunable stacking fault energies by tailoring local chemical order in CrCoNi medium-entropy alloys, Proc. Natl. Acad. Sci. USA **115**, 8919 (2018).

[14] Q.-J. Li, H. Sheng, and E. Ma, Strengthening in multi-principal element alloys with local-chemical-order roughened dislocation pathways, Nat. Commun. **10**, 3563 (2019).

[15] P. A. Santos-Florez, S.-C. Dai, Y. Yao, H. Yanxon, L. Li, Y.-J. Wang, Q. Zhu, and X.-X. Yu, Short-range order and its impacts on the BCC MoNbTaW multi-principal element alloy by the machine-learning potential, Acta Mater. **255**, 119041 (2023).

[16] P. Yu, J. P. Du, S. Shinzato, F. S. Meng, and S. Ogata, Theory of history-dependent multi-layer generalized stacking

fault energy—A modeling of the micro-substructure evolution kinetics in chemically ordered medium-entropy alloys, Acta Mater. **224**, 117504 (2022).

[17] X. Chen *et al.*, Direct observation of chemical short-range order in a medium-entropy alloy, Nature (London) **592**, 712 (2021).

[18] Q. Ding *et al.*, Tuning element distribution, structure and properties by composition in high-entropy alloys, Nature (London) **574**, 223 (2019).

[19] D. B. Miracle and O. N. Senkov, A critical review of high entropy alloys and related concepts, Acta Mater. **122**, 448 (2017).

[20] Z. Su *et al.*, Enhancing the radiation tolerance of high-entropy alloys via solute-promoted chemical heterogeneities, Acta Mater. **245**, 118662 (2023).

[21] Y. Z. Wang and Y. J. Wang, Disentangling diffusion heterogeneity in high-entropy alloys, Acta Mater. **224**, 117527 (2022).

[22] J. Dąbrowa and M. Danielewski, State-of-the-art diffusion studies in the high entropy alloys, Metals (Basel) **10**, 347 (2020).

[23] J. Kottke *et al.*, Experimental and theoretical study of tracer diffusion in a series of (CoCrFeMn)$_{100-x}$Ni$_x$ alloys, Acta Mater. **194**, 236 (2020).

[24] M. Vaidya, S. Sen, X. Zhang, L. Frommeyer, Ł. Rogal, S. Sankaran, B. Grabowski, G. Wilde, and S. V. Divinski, Phenomenon of ultra-fast tracer diffusion of Co in HCP high entropy alloys, Acta Mater. **196**, 220 (2020).

[25] R. Wang, W. Chen, J. Zhong, and L. Zhang, Experimental and numerical studies on the sluggish diffusion in face centered cubic Co-Cr-Cu-Fe-Ni high-entropy alloys, J. Mater. Sci. Technol. **34**, 1791 (2018).

[26] Z. Fan, B. Xing, and P. Cao, Predicting path-dependent diffusion barrier spectra in vast compositional space of multi-principal element alloys via convolutional neural networks, Acta Mater. **237**, 118159 (2022).

[27] A. Dash, A. Paul, S. Sen, S. Divinski, J. Kundin, I. Steinbach, B. Grabowski, and X. Zhang, Recent advances in understanding diffusion in multiprincipal element systems, Annu. Rev. Mater. Res. **52**, 383 (2022).

[28] B. Xing, X. Wang, W. J. Bowman, and P. Cao, Short-range order localizing diffusion in multi-principal element alloys, Scr. Mater. **210**, 114450 (2022).

[29] S. Zhao, Role of chemical disorder and local ordering on defect evolution in high-entropy alloys, Phys. Rev. Mater. **5**, 10364 (2021).

[30] B. Xing, W. Zou, T. J. Rupert, and P. Cao, Vacancy diffusion barrier spectrum and diffusion correlation in multicomponent alloys, Acta Mater. **266**, 119653 (2024).

[31] D. de Fontaine, The number of independent pair-correlation functions in multicomponent systems, J. Appl. Crystallogr. **4**, 15 (1971).

[32] Y.-J. Wang, G.-J. J. Gao, and S. Ogata, Atomistic understanding of diffusion kinetics in nanocrystals from molecular dynamics simulations, Phys. Rev. B **88**, 115413 (2013).

[33] K. Y. Tsai, M. H. Tsai, and J. W. Yeh, Sluggish diffusion in Co-Cr-Fe-Mn-Ni high-entropy alloys, Acta Mater. **61**, 4887 (2013).

[34] M. Vaidya, K. G. Pradeep, B. S. Murty, G. Wilde, and S. V. Divinski, Bulk tracer diffusion in CoCrFeNi and CoCrFeMnNi high entropy alloys, Acta Mater. **146**, 211 (2018).

[35] S. C. Dai, Z. C. Xie, and Y. J. Wang, Atomistic interpretation of extra temperature and strain-rate sensitivity of heterogeneous dislocation nucleation in a multi-principal-element alloy, Int. J. Plast. **149**, 103155 (2022).

[36] S. Plimpton, Fast parallel algorithms for short-range molecular dynamics, J. Comput. Phys. **117**, 1 (1995).

[37] A. Stukowski, Visualization and analysis of atomistic simulation data with OVITO–the open visualization tool, Model Simul. Mater. Sci. Eng. **18**, 15012 (2009).